scenario, the average INR of every CCI signal that impacts the (1, 2)th and the (2, 2)th hops, i.e., $\bar{\gamma}_{I_{1,2}}$ and $\bar{\gamma}_{2,2}$, respectively, is equal to $\text{INR}_2 = 0.005E_T/N_0$. In the second scenario, $\bar{\gamma}_{I_{1,1}}$ and $\bar{\gamma}_{I_{2,1}}$ are equal to $\text{INR}_3 = 0.006E_T/N_0$, whereas $\bar{\gamma}_{I_{1,2}}$ and $\bar{\gamma}_{2,2}$ are equal to $\text{INR}_4 = 0.002E_T/N_0$. As observed, the adaptive power-allocation algorithm outperforms the equal-power-allocation scheme. Moreover, the optimal power solution has a very little impact on the system error performance in the low E_T/N_0 range. This is because of the fact that, in the low E_T/N_0 range, AWGN is the most dominant factor on performance. Furthermore, at high E_T/N_0, the error floor in schemes with adaptive power allocation decreases significantly compared with the case with equal power allocation. It is also attested that, as the average INR value decreases, i.e., $\bar{\gamma}_{I_{1,1}}$ and $\bar{\gamma}_{I_{2,1}}$ decrease from $\text{INR}_1 = 0.015E_T/N_0$ to $\text{INR}_3 = 0.006E_T/N_0$ and $\bar{\gamma}_{I_{1,2}}$ and $\bar{\gamma}_{2,2}$ decrease from $\text{INR}_2 = 0.005E_T/N_0$ to $\text{INR}_4 = 0.002E_T/N_0$, the performance of both the adaptive power allocation and the equal-power scheme is improved, as compared with the performance in the interference-free case.

VI. Conclusion

The effect of CCI on the performance of multihop multibranch wireless systems with the AF relaying technique has been studied in this paper. We assumed that the desired signal and all the interfering signals are subject to independent Rayleigh fading. All the interfering signals were presumed to take arbitrary INR values. We obtained exact and upper bound expressions for the end-to-end SINR. Following that, a lower bound on the outage probability was derived in closed form. In addition, we derived approximate expressions for the error and outage probabilities. The analysis is valid for arbitrary numbers of branches, hops, and interferers, and for different average INR values. Finally, aiming at optimizing the system performance in terms of minimizing the error probability, we investigated adaptive power allocation at the source node and all the relays. Correspondingly, we derived closed-form expressions for the energy values of the nodes. Our results verified that, by applying the energy values obtained through the optimization process, the performance of the system can improve significantly. Such optimization is indeed very important for the deployment of relaying networks in practical environments with CCI.

References

[1] V. Asghari, A. Maaref, and S. Aïssa, "Symbol error probability analysis for multihop relaying over Nakagami fading channels," in *Proc. IEEE WCNC*, Sydney, Australia, Apr. 2010, pp. 1–6.

[2] M. O. Hasna and M. S. Alouini, "Outage probability of multi-hop transmission over Nakagami fading channels," *IEEE Commun. Lett.*, vol. 7, no. 5, pp. 216–218, May 2003.

[3] A. Agustin and J. Vidal, "Amplify-and-forward cooperation under interference-limited spatial reuse of the relay slot," *IEEE Trans. Wireless Commun.*, vol. 7, no. 5, pp. 1952–1962, May 2008.

[4] C. Zhong, S. Jin, and K.-K. Wong, "Dual-hop systems with noisy relay and interference-limited destination," *IEEE Trans. Commun.*, vol. 58, no. 3, pp. 764–768, Mar. 2010.

[5] I. Krikidis, J. S. Thompson, S. McLaughlin, and N. Goertz, "Max-min relay selection for legacy amplify-and-forward systems with interference," *IEEE Trans. Wireless Commun.*, vol. 8, no. 6, pp. 3016–3027, Jun. 2009.

[6] S. S. Ikki and S. Aïssa, "Multihop wireless relaying systems in the presence of cochannel interferences: Performance analysis and design optimization," *IEEE Trans. Veh. Technol.*, vol. 61, no. 2, pp. 566–573, Feb. 2012.

[7] J. Liu, N. B. Shroff, and H. D. Sherali, "Optimal power allocation in multi-relay MIMO cooperative networks: Theory and algorithms," *IEEE J. Sel. Areas Commun.*, vol. 30, no. 2, pp. 331–340, Feb. 2012.

[8] Y. Hyungseok and G. L. Stüber, "Outage analysis for general decode-and-forward cooperative relaying systems with co-channel interference," in *Proc. IEEE WCNC*, Paris, France, Apr. 2012, pp. 65–69.

[9] Y. Chen and C. Tellambura, "Distribution function of selection combiner output in equally correlated Rayleigh, Rician, and Nakagami-m fading channels," *IEEE Trans. Commun.*, vol. 52, no. 11, pp. 1948–1956, Nov. 2004.

[10] D. S. Michalopoulos, H. A. Suraweera, G. K. Karagiannidis, and R. Schober, "Amplify-and-forward relay selection with outdated channel estimates," *IEEE Trans. Commun.*, vol. 60, no. 5, pp. 1278–1290, May 2012.

[11] C. Shao-I, "Performance of amplify-and-forward cooperative diversity networks with generalized selection combining over Nakagami-m fading channels," *IEEE Commun. Lett.*, vol. 16, no. 5, pp. 634–637, May 2012.

[12] M. Seyfi, S. Muhaidat, and L. Jie, "Amplify-and-forward selection cooperation over Rayleigh fading channels with imperfect CSI," *IEEE Trans. Wireless Commun.*, vol. 11, no. 1, pp. 199–209, Jan. 2012.

[13] A. Papoulis and S. U. Pillai, *Random Variables and Stochastic Processes*, 4th ed. New York, NY, USA: McGraw-Hill, 2002.

[14] Z. Wang and G. B. Giannakis, "A simple and general parameterization quantifying performance in fading channels," *IEEE Trans. Commun.*, vol. 51, no. 8, pp. 1389–1398, Aug. 2003.

[15] A. Ribeiro, X. Cai, and G. B. Giannakis, "Symbol error probabilities for general cooperative links," *IEEE Trans. Wireless Commun.*, vol. 4, no. 3, pp. 1264–1273, May 2005.

EVM Analysis for Broadband OFDM Direct-Conversion Transmitters

F. Gregorio, *Member, IEEE*, J. Cousseau, *Senior Member, IEEE*, S. Werner, *Senior Member, IEEE*, T. Riihonen, *Student Member, IEEE*, and R. Wichman

***Abstract*—Low-cost orthogonal frequency-division multiplexing (OFDM) direct-conversion transceivers suffer from signal degradation through the impairments of the analog front end, e.g., due to in-phase and quadrature (IQ) imbalance, phase noise, and nonlinear power amplifier (PA) effects. This paper analyzes joint performance degradation due to these key transmitter imperfections. Error vector magnitude (EVM) is chosen as the figure of merit, which is motivated by its frequent use in the standards for specifying transmitter requirements. In particular, we derive closed-form EVM expressions for the challenging problem of wideband OFDM transmitter design and validate the analysis through simulations. Based on the study, it is possible to conclude that EVM is governed by the memory effects associated with the PA and the reciprocal of the image rejection ratio (IRR), which is defined by the IQ modulator. We also demonstrated that intercarrier interference (ICI) due to the local oscillator phase noise shows an approximately frequency-flat response.**

***Index Terms*—Analog front-end, error vector magnitude, IQ imbalance, nonlinear amplification, orthogonal frequency-division multiplexing (OFDM), phase noise, radio-frequency (RF) impairments.**

Manuscript received July 13, 2012; revised November 29, 2012 and February 4, 2013; accepted February 19, 2013. Date of publication March 7, 2013; date of current version September 11, 2013. This work was supported in part by the Agencia Nacional de Promoción Científica y Tecnológica under PICT 2008-00104 and PICT 2008-0182; by the Universidad Nacional del Sur, Argentina, under Project 24/K044; by the Academy of Finland, and by Centre of Excellence in Smart Radios and Wireless Research. The review of this paper was coordinated by Prof. Y. R. Zheng.

F. Gregorio and J. Cousseau are with the Consejo Nacional de Investigaciones Científicas y Técnicas—Department of Electrical and Computer Engineering, Universidad Nacional del Sur, Bahía Blanca, Argentina.

S. Werner, T. Riihonen, and R. Wichman are with the Department of Signal Processing and Acoustics, Aalto University School of Electrical Engineering, 00076 Espoo, Finland.

Color versions of one or more of the figures in this paper are available online at http://ieeexplore.ieee.org.

Digital Object Identifier 10.1109/TVT.2013.2250534

I. Introduction

The design of compact and low-cost user terminals for future wireless systems is a very difficult problem, because the requirements of flexibility and reconfigurability prevent the use of dedicated hardware, which is designed and optimized for one particular application. It is necessary to satisfy the strict constraints on the size and cost of the individual radios [1]. Emerging communication technologies require high spectral efficiency and robustness against time-dispersive channels. For this reason, orthogonal frequency-division multiplexing (OFDM) has been adopted in the majority of wireless communication standards [2]. Despite several advantages, OFDM is sensitive to different system distortion sources associated with the radio-frequency (RF) front end. Feasible low-cost technologies are employed to keep the cost and size of mass-market implementations low. However, the use of low-cost components creates several imperfections/impairments that degrade system performance, e.g., power amplifiers (PAs) with nonlinear response [3], inaccurate local oscillators (LOs) [4], and mismatches in the I and Q branches of direct-conversion transceivers [5].

The degradation that each RF impairment introduces on the system performance can be quantified by studying the error vector magnitude (EVM), which provides adequate information regarding in-band distortion generated by each transceiver block and is widely adopted in communication standards [2], [6]. It is customary to specify the maximum allowable EVM value as a function of constellation size and code rate. Several performance figures related to different RF impairments have been addressed in earlier works, where the individual effects of each imperfection are considered. Analytical results for IQ imbalance and nonlinear distortion (NLD) at the transmitter front end are obtained in [7] for narrow-band (frequency-independent) systems. EVM expressions for IQ imbalance and phase noise are derived for single-carrier systems in [8] and OFDM systems in [9]. Performance degradation due to nonlinear PA distortion is investigated in [10]. System performance degradation due to phase noise is addressed in [4] and [11]. In addition, the effects of carrier frequency offset and phase noise in single- and multicarrier systems are evaluated in [12]. Simulation results for a single-carrier *long term evolution* (LTE) transceiver considering nonlinear PA, IQ imbalance, and phase noise are presented in [13].

On the other hand, the impact of phase noise, IQ imbalance, and nonlinearities in multiple-antenna OFDM systems is presented in [14]. In this paper, only simulation results are reported, and memory effects are not contemplated. A closed-form expression of the effective signal-to-interference ratio for a multiantenna OFDM system affected by frequency-selective IQ imbalance is derived in [15]. The effects of phase noise and nonlinear amplification are not included in this analysis.

In this paper, we derive closed-form EVM expressions for a wireless OFDM transmitter considering the following RF impairments: transmitter IQ imbalance, nonlinear PA distortion, and phase noise introduced by the LO. To the best of our knowledge, there are no contributions addressing analytical expressions for EVM combining all these effects. Furthermore, the more challenging problem of impairment effects in broadband systems is considered in our analysis, which require frequency-dependent models.

This paper is outlined as follows: In Section II, a brief discussion of the OFDM transmitter and the main RF front-end impairments considered is presented. The EVM is evaluated in Section III considering the joint effects of transmitter IQ imbalance, nonlinear PA distortion, and LO phase noise. Numerical examples are presented in Section IV to illustrate the accuracy of the closed-form expressions. Finally, conclusions are presented in Section V.

II. Orthogonal Frequency-Division Multiplexing Transmitter with Imperfections

A typical OFDM transmitter has two essential blocks: a digital block that operates at baseband frequency and an RF front-end block that operates at RF. These two blocks are interfaced by digital-to-analog converters (DACs). Several impairments of the RF front end affect the OFDM system performance. In our analysis, we consider the effects of transmitter IQ imbalance, phase noise, and nonlinear PA distortion. The DAC resolution is chosen to provide sufficient dynamic range such that distortion due to quantization and clipping is negligible.

The OFDM system under consideration has N subcarriers. Let $X[k] \in \mathcal{C}$ denote the modulated data symbol associated with subcarrier k. The time-domain OFDM symbols $\{x[n]\}_{n=0}^{N-1}$ are obtained via the inverse discrete Fourier transform (IDFT), i.e., $x[n] = (1/\sqrt{N}) \sum_{k=0}^{N-1} X[k] e^{j(2\pi/N)kn}, n = 0, 1, \ldots, N-1$. After the IDFT, a cyclic prefix is added to the transmitted block $\{x[n]\}_{n=0}^{N-1}$. The OFDM signal is converted into a continuous-time (complex) baseband signal, i.e., $x(t)$, with in-phase (I) and quadrature (Q) components $x_{\mathrm{i}}(t)$ and $x_{\mathrm{q}}(t)$. These component signals are filtered by low-pass filters, i.e., $h_{\mathrm{i}}(t)$ and $h_{\mathrm{q}}(t)$, that model the cascade of DACs and the analog filters employed to eliminate Nyquist images and noise. Impulse responses $h_{\mathrm{i}}(t)$ and $h_{\mathrm{q}}(t)$ are, in general, different, creating frequency-dependent IQ mismatch. IQ components at the low-pass filters' output (continuous-time baseband signals) are directly modulated to RF using two carrier signals of frequency f_c from the LO that are ideally orthogonal. However, considering practical implementations and in addition to phase noise effects [17], LO signals present phase and amplitude imbalance between the IQ branches [16].

The continuous-time passband signal can be written as

$$\tilde{x}_{\mathrm{rf}}(t) = \left(x_{\mathrm{i}}(t) \otimes h_{\mathrm{i}}(t)\right) c_{\mathrm{i}}(t) - \left(x_{\mathrm{q}}(t) \otimes h_{\mathrm{q}}(t)\right) c_{\mathrm{q}}(t) \tag{1}$$

where $\otimes$ denotes convolution, and the IQ carrier signals, including IQ mismatch and LO phase noise, are given by

$$\begin{aligned} c_{\mathrm{i}}(t) &= \cos\left(2\pi f_c t + \phi(t)\right) \\ c_{\mathrm{q}}(t) &= \beta \sin\left(2\pi f_c t + \theta + \phi(t)\right) \end{aligned} \tag{2}$$

where θ and β are, respectively, the phase and amplitude imbalance between IQ branches, and $\phi(t)$ represents phase noise. By replacing (3) in (1)

$$\begin{aligned} \tilde{x}_{\mathrm{rf}}(t) = {} & \left(x_{\mathrm{i}}(t) \otimes h_{\mathrm{i}}(t)\right) \cos\left(2\pi f_c t + \phi(t)\right) \\ & - \left(x_{\mathrm{q}}(t) \otimes h_{\mathrm{q}}(t)\right) \beta \sin\left(2\pi f_c t + \theta + \phi(t)\right). \end{aligned} \tag{3}$$

Using $\sin(A+B) = \sin(A)\cos(B) + \sin(B)\cos(A)$ and Euler's theorem

$$\begin{aligned} \tilde{x}_{\mathrm{rf}}(t) = {} & \left(x_{\mathrm{i}}(t) \otimes h_{\mathrm{i}}(t)\right) \cos\left(2\pi f_c t + \phi(t)\right) - \left(x_{\mathrm{q}}(t) \otimes h_{\mathrm{q}}(t)\right) \\ & \times \beta \left[\sin\left(2\pi f_c t + \phi(t)\right) \cos(\theta) \right. \\ & \left. + \sin(\theta) \cos\left(2\pi f_c t + \phi(t)\right)\right] \\ = {} & \left(x_{\mathrm{i}}(t) \otimes h_{\mathrm{i}}(t) - \left(x_{\mathrm{q}}(t) \otimes h_{\mathrm{q}}(t)\right) \beta \frac{e^{j\theta} - e^{-j\theta}}{2j}\right) \\ & \times \frac{e^{j(2\pi f_c t + \phi(t))} + e^{-j(2\pi f_c t + \phi(t))}}{2} \\ & - \left(\left(x_{\mathrm{q}}(t) \otimes h_{\mathrm{q}}(t)\right) \beta \frac{e^{j\theta} + e^{-j\theta}}{2}\right) \\ & \times \frac{e^{j(2\pi f_c t + \phi(t))} - e^{-j(2\pi f_c t + \phi(t))}}{2j}. \end{aligned}$$

By defining

$$g_1(t) = \frac{1}{2}\left(h_{\rm i}(t) + \beta e^{j\theta} h_{\rm q}(t)\right)$$
$$g_2(t) = \frac{1}{2}\left(h_{\rm i}(t) - \beta e^{j\theta} h_{\rm q}(t)\right) \quad (4)$$

and using $x_{\rm i}(t) = (x(t) + x^*(t))/2$ and $x_{\rm i}(t) = (x(t) - x^*(t))/2$, the real passband signal at the output of the modulator can be expressed as

$$\begin{aligned}\tilde{x}_{\rm rf}(t) =& \left(g_1(t) \otimes x(t) + g_2(t) \otimes x^*(t)\right) \frac{e^{j(2\pi f_c t + \phi(t))}}{2} \\ &+ \left(g_1(t) \otimes x(t) + g_2(t) \otimes x^*(t)\right)^* \frac{e^{-j(2\pi f_c t + \phi(t))}}{2} \\ =& \Re\left\{\left(g_1(t) \otimes x(t) + g_2(t) \otimes x^*(t)\right) e^{j(\phi(t) + 2\pi f_c t)}\right\} \quad (5)\end{aligned}$$

where $(\cdot)^*$ denotes complex conjugation. The baseband equivalent at the output of the mixer with IQ imbalance and phase noise is then

$$x_{\rm rf}(t) = \left(g_1(t) \otimes x(t) + g_2(t) \otimes x^*(t)\right) e^{j\phi(t)}. \quad (6)$$

After upconversion, the signal is amplified by a broadband PA with input–output model $p(\cdot)$. The signal at the PA output is then expressed by

$$\begin{aligned}x_{\rm tx}(t) =& \, p\left(x_{\rm rf}(t)\right) \\ =& \, p\left(\left(g_1(t) \otimes x(t) + g_2(t) \otimes x^*(t)\right) e^{j\phi(t)}\right). \quad (7)\end{aligned}$$

Finally, at the receiver side, the signal is downconverted, filtered, and sampled to recover the original symbols. Assuming an ideal demodulator, the signal is sampled at period T, which gives $x_{\rm tx}[n] = x_{\rm tx}(nT) = p(x_{\rm rf}[n])$.

In this paper, the PA is modeled as a Wiener structure [18], which is a frequently employed model formed by linear filter $h_{\rm pa}[n]$ followed by static nonlinearity $g(\cdot)$. The discrete-time baseband PA output signal can be written as

$$\begin{aligned}x_{\rm tx}[n] =& \, g\left(x_{\rm rf}[n] \otimes h_{\rm pa}[n]\right) \\ =& \, K_L\left(x_{\rm rf}[n] \otimes h_{\rm pa}[n]\right) + d[n] \\ =& \, K_L\left(\left(g_1[n] \otimes x[n] + g_2[n] \otimes x^*[n]\right) e^{j\phi[n]}\right) \\ & \otimes h_{\rm pa}[n] + d[n] \quad (8)\end{aligned}$$

where we use the extended version of Bussgang's theorem [19] to represent the effects of NLD as a sum of two uncorrelated components. The first term is just a scaled version of the filtered input signal ($K_L \leq 1$), whereas $d[n]$ is an additive distortion term. In the last expression, $\phi[n] = \phi(nT_s/N)$ represents the nth sample of the phase noise value within the OFDM symbol.

The equivalent frequency-domain baseband signal at subcarrier k is obtained by applying the discrete Fourier transform (DFT) to (9), i.e.,

$$\begin{aligned}X_{\rm tx}[k] = K_L\left(\left(G_1[k]X[k] + G_2[k]X^{\#}[k]\right) \otimes \Phi[k]\right) \\ \times H_{\rm pa}[k] + D[k] \quad (9)\end{aligned}$$

where $X^{\#}[k] = X^*[N-k]$ represents the mirrored OFDM symbol [5] obtained from the frequency-domain representation of $\mathbf{x}[n]$ and $\mathbf{x}^*[n]$ $N \times 1$ vectors. Mirror signal attenuation can be quantified by the *image rejection ratio* (IRR) defined by $IRR[k] = 10\log_{10}((|G_1[k]|^2/|G_2[k]|^2))$ [15]. The IRR represents degradation due to the upconverter block (including phase and amplitude imbalance of the IQ modulator and impulse response mismatch). In the case of perfectly balanced signals, i.e., $G_2[k] = 0$, the IRR tends to ∞, given an infinite attenuation of the image signal.

The frequency-domain representation of the phase noise process is given by

$$\Phi[k] = \frac{1}{N}\sum_{m=0}^{N-1} e^{j\phi_m[n]} e^{-j\frac{2\pi}{N}km}. \quad (10)$$

The demodulated signal can be expressed as

$$\begin{aligned}X_{\rm tx}[k] = K_L\Bigg(&\sum_{l=0}^{N-1} G_1[l]X[l]\Phi[k-l] \\ &+ \sum_{l=0}^{N-1} G_2[l]X^*[N-l]\Phi[k-l]\Bigg) H_{\rm pa}[k] + D[k] \quad (11)\end{aligned}$$

where $H_{\rm pa}[k]$ represents the frequency response at subcarrier k of linear filter $h_{\rm pa}[n]$ associated with the Wiener PA model. The phase noise effects can be separated into a common phase error (CPE) term and an intercarrier interference (ICI) term [4]. Equation (11) can now be written as

$$\begin{aligned}X_{\rm tx}[k] = H'_{\rm pa}[k]\,(&G_1[k]\Phi[0]X[k] + \Gamma[k]G_1[k] \\ &+ G_2[k]X^{\#}[k]\Phi[0] + \Gamma^{\#}[k]G_2[k]\big) + D[k] \quad (12)\end{aligned}$$

where $H'_{\rm pa}[k] = K_L H_{\rm pa}[k]$, $\Phi[0]$ is the CPE term, and $\Gamma[k] = \sum_{l=0, l\neq k}^{N-1} X[l]\Phi[k-l]$ and $\Gamma^{\#}[k] = \Gamma^*[N-k]$ represent the ICI at subcarrier k arising from neighboring and mirrored subcarriers, respectively.

III. Error Vector Magnitude Analysis

Here, we derive a closed-form expression of the resulting EVM of a wideband OFDM transmitter subject to RF impairments. The EVM at subcarrier k, i.e., $\xi[k]$, is expressed using a normalized difference between the original constellation points, i.e., $X[k]$, and the recovered signal affected by system imperfections, as defined by [20]

$$\xi[k] = \sqrt{\frac{E\left[|e[k]|^2\right]}{E\left[|X[k]|^2\right]}} \quad (13)$$

where $E[\cdot]$ denotes the expectation. The effective signal-to-noise ratio ($SNR_{\rm eff}$) is another useful figure of merit and is related to EVM as $\xi[k] = SNR_{\rm eff}[k]^{-1/2}$.

Error signal $e[k]$ is defined as the difference between the original signal and the received signal after downconversion and zero-forcing equalization of the impairments. That is, we have

$$e[k] = X[k] - \frac{X_{\rm tx}[k]}{Z_{\rm eq}[k]} \quad (14)$$

where $X_{\rm tx}[k]$ is given in (12), and $Z_{\rm eq}[k]$ is the zero-forcing equalizer coefficient at subcarrier k. We assume that the equalizer coefficient is obtained using a channel estimation technique that estimates the multiplication of the CPE term, $\Phi[0]$ and IQ modulator and PA filters, $H'_{\rm pa}[k]G_1[k]$ of each OFDM symbol by using a set of transmitted pilots. Signal $X_{\rm tx}[k]$ can be written as

$$X_{\rm tx}[k] = H'_{\rm pa}[k]G_1[k]\Phi[0]X[k] + \varsigma[k] \quad (15)$$

where $\varsigma[k]$ is the total system noise that includes PA distortion, ICI, and interference from mirror subcarriers. Assuming a perfect estimate of the cascade $H'_{\rm pa}[k]G_1[k]\Phi[0]$, the equalizer estimates for a set of known pilot symbols is given by $Z_{\rm eq}[k] = H'_{\rm pa}[k]G_1[k]\Phi[0]$, and the error signal after equalization can be written as

$$e[k] = X[k] - \frac{X_{\rm tx}[k]}{Z_{\rm eq}[k]}$$
$$= \frac{\Gamma[k]}{\Phi[0]} + \frac{G_2[k]X^{\#}[k]}{G_1[k]} + \frac{\Gamma^{\#}[k]G_2[k]}{G_1[k]\Phi[0]} + \frac{D[k]}{H'_{\rm pa}[k]G_1[k]\Phi[0]}. \quad (16)$$

Then, the mean-square-error signal can be written as

$$\begin{aligned} E\left[|e[k]|^2\right] &= E\left[|\Phi[0]|^{-2}\right] \\ &\quad \times \left(E\left[|\Gamma[k]|^2\right] + \frac{|G_2[k]|^2}{|G_1[k]|^2} E\left[\left|\Gamma^{\#}[k]\right|^2\right] \right. \\ &\quad \left. + \frac{E\left[|D[k]|^2\right]}{\left|H'_{\rm pa}[k]\right|^2 |G_1[k]|^2} \right) \\ &\quad + \frac{|G_2[k]|^2}{|G_1[k]|^2} E\left[\left|X^{\#}[k]\right|^2\right] \\ &\approx \left(\sigma_\gamma^2[k] + \frac{|G_2[k]|^2}{|G_1[k]|^2}\sigma_\gamma^2[N-k] \right. \\ &\quad \left. + \frac{\sigma_D^2[k]}{\left|H'_{\rm pa}[k]\right|^2 |G_1[k]|^2} \right) \\ &\quad + \frac{|G_2[k]|^2}{|G_1[k]|^2}\sigma_x^2 \end{aligned} \quad (17)$$

where $\sigma_\gamma^2[k] = E[|\Gamma[k]|^2]$, $\sigma_\gamma^2[N-k] = \sigma_\gamma^{\#^2}[k] = E[|\Gamma^{\#}[k]|^2]$, and $\sigma_D^2[k] = E[|D[k]|^2]$. Note that in our analysis, it is assumed that each subcarrier is modulated with identical constellation size, and no power loading is implemented. In this case, $\sigma_x^2 = \sigma_x^{\#^2} = E[|X^{\#}[k]|^2]$. The approximation in (17) originates from the assumption that $\Phi[0] \approx e^{j\phi_0}$ and, as a consequence, $E[|\Phi[0]|^{-2}] \approx 1$. A more accurate value of $E[|\Phi[0]|^{-2}]$ can be calculated in terms of the moments of the total ICI power. By Parseval's theorem, we have $\sum_{l=0}^{N} |\Phi[l]|^2 = 1$, and the term $|\Phi[0]|^2$ can be calculated by exploiting a series expansion of the relation $|\Phi[0]|^2 = 1 - \sum_{l=1}^{N} |\Phi[l]|^2$. The moments of the total ICI power, for both free-running and PLL-type oscillators, may be evaluated using the results in [21] and [22].

Finally, replacing (17) in (13), the EVM at the kth subcarrier is given by (18), shown at the bottom of the page.

From (18), we can make the following general observations.

- In the case of reduced IQ imbalance ($\beta \approx 1$, $\theta = 0$, and $h_{\rm i} = h_{\rm q}$), ($|G_2[k]|^2/|G_1[k]|^2) \approx 0$ or frequency-independent IQ imbalance ($h_{\rm i} = h_{\rm q}$), the shape of the EVM curve is governed by the NLD whose frequency dependence is defined by the PA memory.
- For large backoff values, the PA-induced NLD will be small, i.e., $\sigma_D^2[k] \approx 0$, and the shape of the EVM curve is defined by the reciprocal of the IRR.
- When the ICI is the dominant impairment, the EVM curve will be frequency flat.

In the following section, we will validate the accuracy of (18) through extensive simulations. For this purpose, we first need to know model-specific parameters $\sigma_\gamma^2[k]$ and $\sigma_D^2[k]$.

A. Calculation of $\sigma_\gamma^2[k]$

The phase-noise-induced ICI power $\sigma_\gamma^2[k]$ depends on the bandwidth of the phase noise process and the subcarrier spacing $B_s = 1/(NT_s)$ [23]. Assuming knowledge of the power spectral density (PSD) of the phase noise process, i.e., $S(f)$, the ICI power can be expressed as [24]

$$\sigma_\gamma^2[k] = \sigma_x^2 \int_{-\infty}^{\infty} \sum_{\substack{n=0 \\ n\neq k}}^{N} {\rm sinc}^2(f/B_s + k - n) S(f) df. \quad (19)$$

Under the condition that all subcarriers are affected by the same ICI power and the difference between central and edge subcarriers is negligible, we may use the following simplified form:

$$\sigma_\gamma^2[k] \approx \sigma_\gamma^2 = \sigma_x^2 \int_{-\infty}^{\infty} \left[1 - {\rm sinc}^2(f/B_s)\right] S(f) df. \quad (20)$$

Obtaining $\sigma_\gamma^2[k]$ using (19) or (20) requires a model of the PSD $S(f)$. We will herein use the following piecewise linear function [25], i.e.,

$$S(f) = \begin{cases} 10^{-a}, & 0 \le f < f_L \\ 10^{-a}\left(\frac{f}{f_L}\right)^{-b}, & f_L \le f < f_p \\ 10^{-c}, & f > f_p \end{cases}$$

where parameter c defines the white phase noise floor; f_L and f_p define the phase-locked loop (PLL) bandwidth and the phase noise bandwidth (region where the noise floor becomes dominant), respectively; a gives the phase noise level near the center frequency; and b gives the noise fall-off rate. The phase noise PSD and the piecewise linear function are shown in Fig. 1(a).

The LO signal quality is specified by the *integrated single-sideband phase noise* (IPN), which is given by $IPN = \int_0^\infty S(f) df$ (in dBc) [29]. Moreover, the *RMS integrated phase error* $I_{\rm rms} = (180/\pi)\sqrt{2IPN}$ specified in degrees can be also employed.

Fig. 1(b) shows the ICI variance, i.e., σ_γ^2, for an LO with an IPN power of -32 dBc and an error floor of -130 dBc for three different loop bandwidths ($f_L = 5$ kHz, $f_L = 10$ kHz, and $f_L = 20$ kHz) considering an OFDM system with 1024 subcarriers and intercarrier spacing of 15 kHz. The variance was calculated using (19) and the approximation in (20). We see that the ICI variance increases for larger PLL bandwidths and that the difference in ICI variance between borders and central subcarriers is around 3 dB. In Section IV, we verified that this gap gives a difference in terms of EVM that can be considered negligible.

$$\xi[k] = \sqrt{\frac{1}{\sigma_x^2}\left(\sigma_\gamma^2[k] + \frac{|G_2[k]|^2}{|G_1[k]|^2}\sigma_\gamma^2[N-k] + \frac{\sigma_D^2[k]}{\left|H'_{\rm pa}[k]\right|^2 |G_1[k]|^2}\right) + \frac{|G_2[k]|^2}{|G_1[k]|^2}} \quad (18)$$

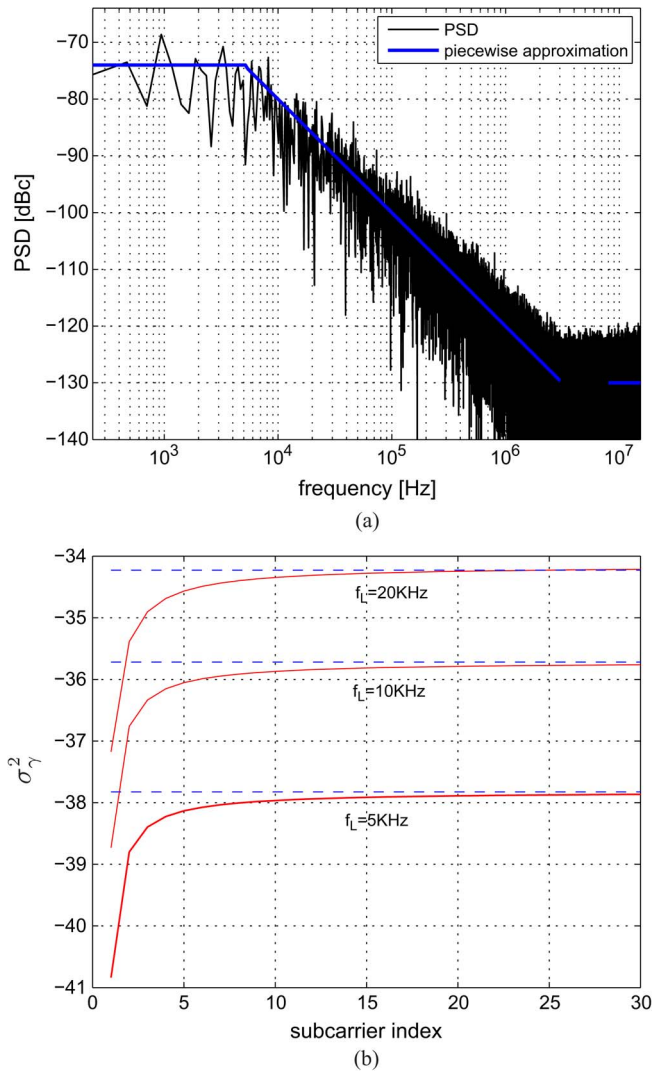

Fig. 1. (a) PSD of the true phase noise and the piecewise linear approximation with the following parameters: $f_L = 5$ kHz; $f_p = 5$ MHz; $a = 7\,4$; $b = 2$; and $c = 13$. (b) ICI variance, i.e., σ^2_γ, of an LO with an IPN power of -32 dBc and an error floor of -130 dBc for loop bandwidths $f_L = 5$ kHz, $f_L = 10$ kHz, and $f_L = 20$ kHz. The subcarrier spacing is 15 kHz. ICI variance values calculated using frequency-flat approximation [see (20)] and frequency-selective ICI [see (19)] are plotted in dotted and solid lines, respectively.

B. Calculation of $\sigma^2_D[k]$

The nonlinear PA is approximated by a Wiener model. The static nonlinearity is modeled with a kth-order polynomial, and the linear filter is modeled by an FIR filter of order L_a. The PA output can be written as [27]

$$x_{\rm tx}[n] = \sum_{\substack{i=3\\ \text{odd}}}^{K} c_i x'_{\rm rf}[n]\,|x'_{\rm rf}[n]|^{i-1} \tag{21}$$

where $x'_{\rm rf}[n] = \nu x_{\rm rf}[n] \otimes h_{\rm pa}[n]$ is the output of the linear block, and ν is the input backoff (IBO), which scales the symbols to reduce in-band distortion. A large value of the IBO reduces the nonlinear PA distortion, thus reducing the associated performance penalty at the price of reduced power efficiency, because the dynamic range is decreased. The expression obtained for the variance of NLD $\sigma^2_D[k]$, which is derived in the Appendix, is given by

$$\begin{aligned}\sigma^2_D[k] &= \frac{1}{|c_1|^2} E\Bigg[\sum_{p=-L_H+1}^{L_H-1}\sum_{\substack{i=3\\ \text{odd}}}^{K}\sum_{\substack{w=3\\ \text{odd}}}^{K} c_i c_w^* \nu^{i+w} \sum_{l_1=0}^{L_H-1} x[l_1]\bar{h}[l_1] \\ &\quad \times \prod_{r=1}^{(i-1)/2}\left(\sum_{l_{r+1}=0}^{L_H-1} x[l_{r+1}]\bar{h}[l_{r+1}] \sum_{l_{r+2}=0}^{L_H-1} x^*[l_{r+2}]\bar{h}^*[l_{r+2}]\right) \\ &\quad \times \sum_{j_1=0}^{L_H-1} x^*[j_1-p]\bar{h}^*[j_1] \prod_{s=1}^{(w-1)/2}\left(\sum_{j_{s+1}=0}^{L_H-1} x[j_{s+1}-p]\bar{h}[j_{s+1}]\right. \\ &\quad \left.\times \sum_{j_{s+2}=0}^{L_H-1} x^*[j_{s+2}-p]\bar{h}^*[j_{s+2}]\right) e^{-j\frac{2\pi}{N-1}kp}\Bigg]\end{aligned} \tag{22}$$

where $\bar{h}[n]$ is a filter of length L_H that models the cascade $g_1[n] \otimes h_{\rm pa}[n]$.

From (22), we can infer the following.

- For $x[n]$ following a Gaussian distribution with zero mean, nonzero expectation is obtained if for each value of $x[m]$, there is $x^*[j]$ with $m = j$. If this condition is not verified, $E[|D[k]|^2] = 0$. In our analysis, it is assumed that each subcarrier is modulated with identical constellation size, and no power loading is employed. In this case, the Gaussian assumption for the OFDM signal is verified.
- For a memoryless system, i.e., $L_H = 1$, the NLD is frequency flat, and (22) reduces to

$$\begin{aligned}\sigma^2_D[k] &= \sigma^2_D \\ &= \frac{1}{|c_1|^2}\sum_{\substack{i=3\\ \text{odd}}}^{K}\sum_{\substack{w=3\\ \text{odd}}}^{K} c_i c_w^* \nu^{i+w} \\ &\quad E\left[x[n]\,|x[n]|^{i-1}\,x^*[n]\,|x[n]|^{w-1}\right] \\ &= \frac{1}{|c_1|^2}\sum_{\substack{i=3\\ \text{odd}}}^{K}\sum_{\substack{w=3\\ \text{odd}}}^{K} c_i c_w^* \nu^{i+w} E\left[|x[n]|^{i+w}\right].\end{aligned} \tag{23}$$

For illustrative purposes, a simple closed-form expression for the variance of NLD $\sigma^2_D[k]$ can be obtained if the static nonlinearity is modeled with a third-order polynomial, and the filter length verifies $L_H \leq 3$. In this case, the distortion due to PA is given by

$$\begin{aligned}\sigma^2_D[k] = \frac{\nu^4|c_3|^2}{|c_1|^2}\Big(B_0 + 2\text{Re}\{\big(B_{1_1}\bar{h}^*[0]\bar{h}[1] \\ + B_{1_2}\bar{h}^*[1]\bar{h}[2]\big)\,e^{-j\frac{2\pi}{N-1}k}\} + 2\text{Re}\{B_2\bar{h}^*[0]\bar{h}[2]e^{-j\frac{4\pi}{N-1}k}\}\Big)\end{aligned} \tag{24}$$

where B_0, B_{1_1}, B_{1_2}, and B_2 derived in the Appendix are described by (33).

IV. Numerical Results

Here, we compare the EVM from realistic simulations with those obtained analytically. The OFDM system under consideration is based on a Third-Generation Partnership Project Long-Term Evolution (3GPP LTE) downlink-like system and has $N = 1024$ subcarriers modulated with 16-quadrature-amplitude modulation (QAM) data, a

system bandwidth of $B = 10$ MHz, and a sampling frequency of $F_s = 15.36$ MHz, giving subcarrier spacing of 15 kHz. The transmitter front end includes three sources of distortion: IQ imbalance, phase noise from an LO implemented with a PLL, and a nonlinear PA. The other transmitter parameters are based on, but not restricted to, the 3GPP LTE standard, which defines the maximum EVM at the output of the transmitter. In particular, the transmitted signal includes pilot tones to estimate/track the common attenuation and rotation introduced by the channel, IQ imbalance, phase noise, and PA. Frequency/time offset compensation before EVM measurement is also included.

Two PA models are considered in this evaluation: 1) Model 1 is a broadband PA modeled using a Wiener model, where the linear filter is given by $h_{\mathrm{pa1}}(z) = (1 + 0.1z^{-2}/1 - 0.1z^{-1})$ in [26], and the static nonlinearity is modeled by third-order polynomial $g(x) = c_1 x + c_3 x|x|^2$ with coefficients $c_1 = 1.136 + 0.184j$ and $c_3 = -0.3807 - 0.0705j$; and 2) Model 2 is a class-AB PA designed using the Freescale MRF6S23100H laterally diffused metal–oxide–semiconductor device model provided in the ADS component library [27] for a WiMAX/3GPP base station. Its transfer function has been adjusted using a Wiener model. The static nonlinearity is modeled using a seventh-order polynomial with coefficients $c_1 = 0.5804 + 0.0655j$, $c_3 = 0.3678 + 0.0304j$, $c_5 = -0.0855 - 0.0297j$, and $c_7 = 0.0056 + 0.0028j$, and the linear filter is denoted by $h_{\mathrm{pa2}}(z) = 0.8 + 0.216z^{-1} + 0.05z^{-2}$. The phase noise is generated by filtering a Gaussian noise sequence with a filter whose frequency response is defined by the phase noise PSD. In this setup, the adopted phase noise is based on the piecewise linear model described in Section III-A with the following parameters: $f_L = 5$ kHz, $f_c = 50$ MHz, $b = 2$, and $c = 13$. Parameter a is settled as a function of the integrated phase noise (IPN) required.

A. Comparison of Simulations and Analytical Results

The imperfections of the upconversion block are due to phase/amplitude imbalance associated with the modulator, represented by equivalent filters $g_1[n]$ and $g_2[n]$. The mismatch between low-pass filters $h_{\mathrm{i}}[n]$ and $h_{\mathrm{q}}[n]$ can be quantified by impulse response mismatch $b[n]$ defined as $h_{\mathrm{q}}[n] = b[n] \otimes h_{\mathrm{i}}[n]$.

In the following, EVM curves for three different levels of IQ imbalance and PA Model 1 operating with an IBO of -14 dB are studied. EVM results have been evaluated with a phase noise of $I_{\mathrm{rms}} = 2^\circ$ (-32 dBc) in Fig. 2. The analytical results are obtained for both frequency-dependent and frequency-flat ICI effects. The parameters of the IQ modulator under evaluation are Case 1) $\beta = 5\%$, $\theta = 5^\circ$, $b(z) = 1 - 0.05z^{-1}$; Case 2) $\beta = 5\%$, $\theta = 5^\circ$, $b(z) = 1 - 0.03z^{-1}$; and Case 3) $\beta = 5\%$, $\theta = 5^\circ$, $b(z) = 1$. IRR levels from 23 to 32 dB are reported with these values of IQ imbalance and filter mismatch. The theoretical EVM curves are depicted using $\sigma_D^2[k]$ given in (24). Fig. 3 shows the EVM results considering identical IQ modulator parameters and phase noise of $I_{\mathrm{rms}} = 5^\circ$ (-24 dBc): These curves are evaluated using a class-AB PA (Model 2) operating with an IBO of -14 dB. The analytical curves are obtained employing the approximated equation (32) and (30) (numerically solved) to calculate the NLD variance, and the ICI is considered frequency flat. These results show the good match between analytical and simulation results when the approximated equation is employed, even for the case of a PA modeled with large polynomial order.

B. Target EVM

We shall see that the EVM values can be accurately predicted such that the time-consuming simulations are avoided. We will be able to confirm, as detailed in the previous section, that the IQ imbalance

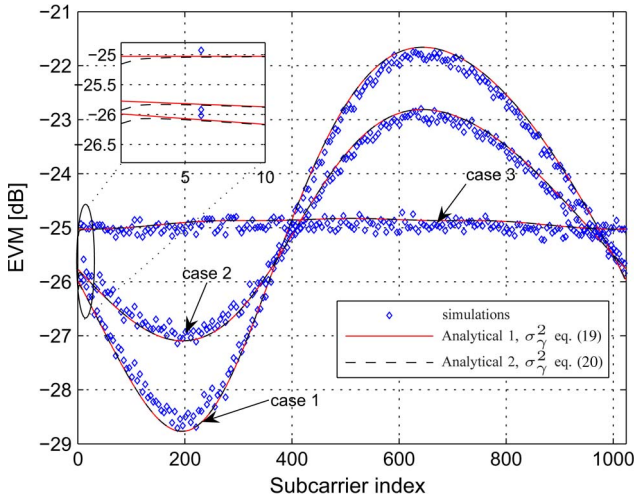

Fig. 2. EVM in three different scenarios. Case 1: $\beta = 5\%$, $\theta = 5^\circ$, $b = 1 - 0.05z^{-1}$. Case 2: $\beta = 5\%$, $\theta = 5^\circ$, $b = 1 - 0.03z^{-1}$. Case 3: $\beta = 5\%$, $\theta = 5^\circ$, $b = 1$. Phase noise I_{rms} is 2° (-32 dBc). The EVM curves are evaluated for PA Model 1 with an operation point set to IBO $= -14$ dB.

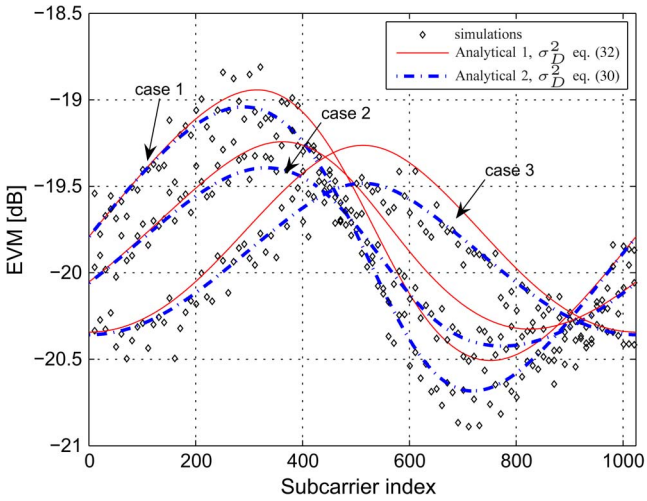

Fig. 3. EVM in three different scenarios. Case 1: $\beta = 5\%$, $\theta = 5^\circ$, $b = 1 - 0.05z^{-1}$. Case 2: $\beta = 5\%$, $\theta = 5^\circ$, $b = 1 - 0.03z^{-1}$. Case 3: $\beta = 5\%$, $\theta = 5^\circ$, $b = 1$. Phase noise I_{rms} is 5° (-24 dBc). The EVM curves are evaluated for PA Model 2 with an operation point set to IBO $= -14$ dB. The analytical curves are obtained employing the approximated equation (32) and (30) (numerically solved) to calculate NLD variance $\sigma_D^2[k]$.

(IRR) and PA memory defines EVM frequency dependence, the ICI can be considered frequency flat by neglecting the effects on the border subcarriers, and the Gaussian assumption for ICI and NLD gives analytical results that accurately match simulations. We analyze the EVM of an RF front end built with off-the-shelf components. For example, the upconverter block can be implemented with quadrature modulator AD8349 from Analog Devices [30]. The AD8349 data sheet specifies an IQ amplitude imbalance $\beta = 0.1$ dB (1.16%) and phase imbalance $\theta = 0.3^\circ$ operating at 2140 MHz. The LO can be implemented with a fractional PLL synthesizer based on ADF4153, resulting in an RMS integrated phase error, i.e., I_{rms}, lower than 0.5°. Assuming the PA is operated with large backoff, the LO and the IQ modulator will give the EVM floor for this particular setup. We assume that the PA is implemented with HMC409LP4 suitable for WiMAX and WLAN (it can be also employed in some operating bands of 3GPP LTE) implementations and extract the Wiener model parameters from the gain and frequency response curves obtained

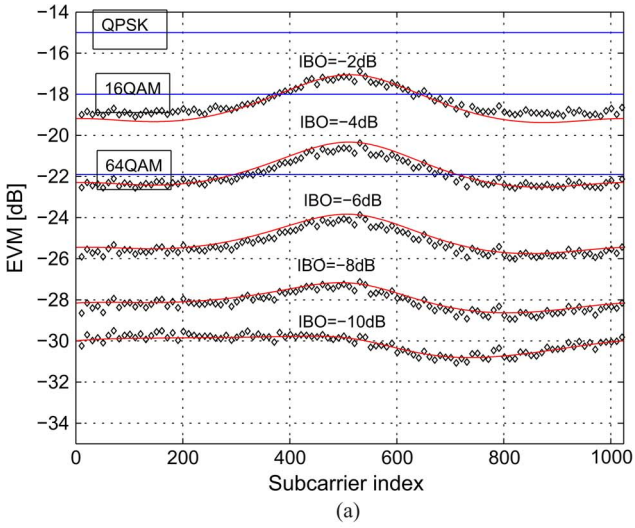

(a)

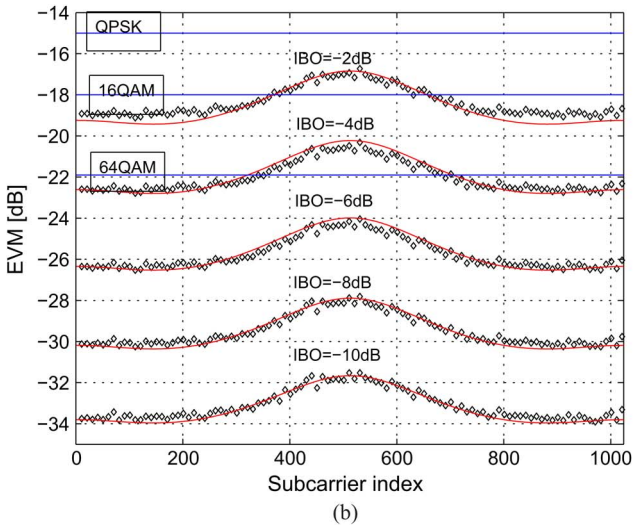

(b)

Fig. 4. (a) and (b) EVM with parameters from the AD8349 data sheet, I/Q imbalance of $\beta = 1.16\%$, and phase imbalance of $\theta = 0.3^\circ$. Phase noise of LO is $I_{\rm rms} = 0.5^\circ$, and the impulse mismatch of I and Q filters is $b = 1 - 0.05z^{-1}$ and $b = 1$ in (a) and (b), respectively. The allowed EVM levels in downlink 3GPP standard when using 64-QAM (-21.9 dB), 16-QAM (-18 dB), and QPSK (-15 dB) are included.

from the manufacturer. The static nonlinearity is modeled using a fifth-order polynomial with coefficients $c_1 = 0.8688$, $c_3 = -0.1018$, and $c_5 = -0.0054$, and the linear filter is denoted by $h_{\rm HMC}(z) = 0.17 + 0.8223z^{-1} - 0.007z^{-2} - 0.0750z^{-3}$.

Fig. 4 shows EVM curves as a function of the PA operation point, i.e., IBO. Impulse mismatch of $b(z) = 1 - 0.05z^{-1}$ and $b(z) = 1$ have been considered in Fig. 4. The figure includes the allowed EVM levels in 3GPP LTE downlink standard when using 64-QAM, 16-QAM, and QPSK modulation. The PA operation point is closely related with the level of mismatch introduced in the upconversion block, and we can infer that a backoff of 6 dB is needed in case of 64-QAM modulation for both cases (with and without impulse mismatch) [see Fig. 4(a) and (b)]. Moving the PA operation point to a more power-efficient region (lower backoff) allows the system to operate with a reduced constellation size (reduced data rate). In case of 16-QAM constellation, the required backoff will be larger than 4 dB.

Fig. 5 shows PA efficiency (PAE), amplifier gain, and output power $P_{\rm o}$ versus input power $P_{\rm i}$ obtained from the PA manufacturer [31] for a typical low-power amplifier (HMC409LP4) used in WiMAX/LTE systems. We see that operating the PA with reduced input power (large

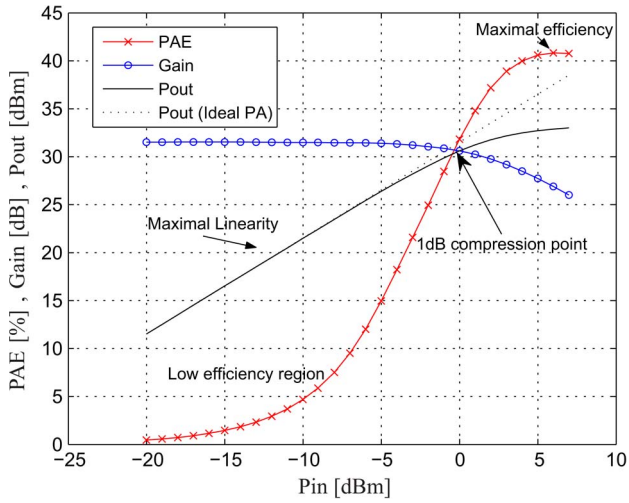

Fig. 5. Efficiency, gain, and transfer function curves of an HMC409LP4 WiMAX/LTE amplifier [31].

backoff) results in a linear response but has a poor PAE. When the PA is operated with IBO $= -6$ dB, the PAE is around 12%. If the backoff is reduced to -4 dB, which is allowed by the reduction in constellation size (reduced data rate), the PAE increases to 18%.

We note that the amplifier backoff needs to be set in a region such that the EVM requirements are satisfied and also that the spectral regrowth satisfies the spectral mask defined by the standards.

The previous results show that the PA NLD and the impairments from the upconverter and LO phase noise can become a limiting factor for the implementation of OFDM transmitters. The power consumption of a PA operating with large backoff should be a conflicting issue particularly for mobile terminals. On the other hand, the minimization of impairments in the upconverter will be useful in reducing the EVM floor that helps relax the admissible levels of NLD. These results motivate the development of compensation techniques for RF impairments, including frequency-dependent behavior that will be an interesting task for the development of future wideband OFDM transceivers.

V. Conclusion

We have analyzed the effects of the most common RF front-end imperfections in an OFDM broadband direct-conversion transmitter. Our closed-form expression for the EVM includes the effects of IQ imbalance, phase noise, and PA nonlinearities. The analytical results, which were validated through extensive simulations, are useful for investigating whether an RF front-end design complies with specifications. In particular, we studied the requirements for the implementation of an LTE transceiver having stringent requirements for EVM levels. We evaluated the tradeoff between distortion due to imperfections in the IQ modulator, the LO, and the PA operation region. EVM expressions can be very useful for radio designers in assessing the system EVM avoiding time-consuming simulations/measurements.

From the derived equations, the designers are able to fix a target EVM and calculate the contribution of each impairment. For example, designers can choose the IQ modulator and the LO circuits and obtain the EVM using the specifications of each component, assuming an ideal PA. The difference between the obtained EVM and the specified EVM is the percentage of allowed distortion assigned to the PA. By using this value, the PA specifications (operation point, output power) can be defined. Impairments due to DACs and any other effects can be modeled as extra thermal noise and employed as a security margin in the design of the transmitter.

APPENDIX
EXPRESSION FOR $\sigma_D^2[k]$

The signal at the PA output can be written as

$$x_{\mathrm{tx}}[n] = \sum_{\substack{i=1 \\ \text{odd}}}^{K} c_i x'_{\mathrm{rf}}[n]\,|x'_{\mathrm{rf}}[n]|^{i-1} \tag{25}$$

where

$$\begin{aligned} x'_{\mathrm{rf}}[n] &= \nu x_{\mathrm{rf}}[n] \otimes h_{\mathrm{pa}}[n] \\ &= h_{\mathrm{pa}}[n] \otimes \left(g'_1[n] \otimes (\nu x[n]) + g'_2[n] \otimes (\nu x^*[n])\right. \\ &\quad \left. + \beta e^{-j\theta}\gamma[n] + \beta e^{-j\theta}\gamma^*[n]\right). \end{aligned} \tag{26}$$

To simplify the analysis, we consider realistic levels of IQ imbalance ($|g'_1|^2 \gg |g'_2|^2$) and phase noise ($\sigma_x^2 \gg \sigma_\gamma^2$). Then, we take into account only the first term of (27), i.e., $g'_1[n] \otimes x[n]$, to obtain

$$\begin{aligned} x'_{\mathrm{rf}}[n] &\approx h_{\mathrm{pa}}[n] \otimes g'_1[n] \otimes (\nu x[n]) \\ &= \nu \bar{h}[n] \otimes x[n] = \nu \sum_{l=0}^{L_H-1} x[n-l]\bar{h}[l] \end{aligned} \tag{27}$$

where $\bar{h}[n] = g_1[n] \otimes h_{\mathrm{pa}}[n]$. The distortion term can be expressed as

$$\begin{aligned} d[n] &= \sum_{\substack{i=3 \\ \text{odd}}}^{K} \frac{c_i}{c_1} x'_{\mathrm{rf}}[n]\,|x'_{\mathrm{rf}}[n]|^{i-1} \\ &= \sum_{\substack{i=3 \\ \text{odd}}}^{K} \frac{c_i}{c_1} \nu^k \sum_{l_1=0}^{L_H-1} x[n-l_1]\bar{h}[l_1] \\ &\quad \prod_{r=1}^{(i-1)/2} \left(\sum_{l_{r+1}=0}^{L_H-1} x[n-l_{r+1}]\bar{h}[l_{r+1}] \right. \\ &\quad \left. \times \sum_{l_{r+2}=0}^{L_H-1} x^*[n-l_{r+2}]\bar{h}^*[l_{r+2}] \right). \end{aligned} \tag{28}$$

The frequency-domain representation of the distortion can be obtained by using the DFT of (29), i.e., $D[k] = \sum_{n=0}^{N-1} d[n] e^{-j\frac{2\pi}{N-1}kn}$. Then, the squared module of $D[k]$ can be written as

$$\begin{aligned} |D[k]|^2 &= \sum_{n=0}^{N-1}\sum_{m=0}^{N-1} d[n]d^*[m] e^{-j\frac{2\pi k(n-m)}{N-1}} \\ &= \sum_{n=0}^{N-1}\sum_{m=0}^{N-1}\sum_{\substack{i=3 \\ \text{odd}}}^{K} \frac{c_i}{c_1}\nu^i \sum_{l_1=0}^{L_H-1} x[n-l_1]\bar{h}[l_1] \\ &\quad \prod_{r=1}^{(i-1)/2} \left(\sum_{l_{r+1}=0}^{L_H-1} x[n-l_{r+1}]\bar{h}[l_{r+1}] \right. \\ &\quad \left. \times \sum_{l_{r+2}=0}^{L_H-1} x^*[n-l_{r+2}]\bar{h}^*[l_{r+2}] \right) \\ &\quad \times \sum_{\substack{w=3 \\ \text{odd}}}^{K} \frac{c_w^*}{c_1^*}\nu^w \sum_{j_1=0}^{L_H-1} x^*[m-j_1]\bar{h}^*[j_1] \\ &\quad \times \prod_{s=1}^{(w-1)/2} \left(\sum_{j_{s+1}=0}^{L_H-1} x^*[m-j_{s+1}]\bar{h}[j_{s+1}]) \right. \\ &\quad \left. \times \sum_{j_{s+2}=0}^{L_H-1} x[m-j_{s+2}]\bar{h}^*[j_{s+2}] \right) \\ &\quad \times e^{-j\frac{2\pi k(n-m)}{N-1}}. \end{aligned} \tag{29}$$

To calculate the expectation of $|D[k]|^2$, we assume that $x[n]$ is Gaussian with zero mean and variance σ_x^2 that verifies $E[x[n]] = 0$, $E[x^*[n]] = 0$, $E[(x[n])^m] = 0$, $E[(x^*[n])^m] = 0$, and $E[|x[n]|^m] = m!!\sigma_x^m$ when m is even. Under this assumption, we can infer that

$$E\left[d[n]d^*[m]\right] \begin{cases} \neq 0, & \text{if } |n-m| \le L_H - 1 \\ = 0, & \text{if } |n-m| > L_H - 1. \end{cases}$$

The expectation of $|D[k]|^2$ can be written as

$$\begin{aligned} &E[|D[k]|^2] \\ &= E\left[\sum_{p=-L_H+1}^{L_H-1} \sum_{\substack{i=3 \\ \text{odd}}}^{K} \sum_{\substack{w=3 \\ \text{odd}}}^{K} \frac{c_i c_w^*}{|c_1|^2}\nu^{i+w} \sum_{l_1=0}^{L_H-1} x[l_1]\bar{h}[l_1] \right. \\ &\quad \times \prod_{r=1}^{(i-1)/2} \left(\sum_{l_{r+1}=0}^{L_H-1} x[l_{r+1}]\bar{h}[l_{r+1}] \right. \\ &\quad \left. \times \sum_{l_{r+2}=0}^{L_H-1} x^*[l_{r+2}]\bar{h}^*[l_{r+2}] \right) \\ &\quad \times \sum_{j_1=0}^{L_H-1} x^*[j_1-p]\bar{h}^*[j_1] \\ &\quad \times \prod_{s=1}^{(w-1)/2} \left(\sum_{j_{s+1}=0}^{L_H-1} x[j_{s+1}-p]\bar{h}[j_{s+1}] \right. \\ &\quad \left. \times \sum_{j_{s+2}=0}^{L_H-1} x^*[j_{s+2}-p]\bar{h}^*[j_{s+2}] \right) \\ &\quad \left. \times e^{-j\frac{2\pi}{N-1}kp} \right]. \end{aligned} \tag{30}$$

A simplified version of this expression can be obtained considering the case when the expectation is nonzero. To this purpose, it is possible to consider the terms $x[l_1]x^*[l_2]\cdots x[l_{(k-1)/(2+1)}]x^*[j_1 - p]x[j_2 - p]\cdots x^*[j_{(w-1)/(2+1)} - p]$. The expectation is nonzero if for each value of nonconjugated $x[i]$, there is $x^*[j]$ with $i = j$. It means that we need to consider two element subsets, which must have an equal time index and different conjugation. In case of identical indexes, i.e., $l_1 = l_2 = \cdots = l_{(i-1)/(2+1)} = (j_1 - p) = (j_2 - p) = (j_{(w-1)/(2+1)} - p)$, the expectation of these terms is given by $E[|x[j_1]|^{i+w}] = (i+w)!!\sigma_x^{i+w}$. If the indexes are combined in pairs, the expectation of the terms can be written as $\prod_{l=1}^{(i+w)/2} E[|x[l]|^2] =$

$\prod_{l=1}^{(i+w)/2} 2!!\sigma_x^2$. A general expression for the combination that gives nonzero expectation can be expressed as

$$E\left[|x[1]|^{i_1}\,|x[2]|^{i_2}\cdots|x[l]|^{k_M}\right]\neq 0$$
$$\text{if } i_1+i_2+\cdots+i_M=i+w \text{ and } i_1,i_2,\ldots,i_M \text{ are even.} \quad (31)$$

In general, (30) can be numerically solved. A closed-form expression can be found if the length of the equivalent filter is restricted to $L_H\leq 3$ and a third-order polynomial is analyzed. For this particular case, the expression for $\sigma_D^2[k]$ can written as

$$\sigma_D^2[k]=\frac{\nu^6|c_3|^2}{|c_1|^2}\Big(B_0+2\text{Re}\{\big(B_{1_1}\bar{h}^*[0]\bar{h}[1]+B_{1_2}\bar{h}^*[1]\bar{h}[2]\big)e^{-j\frac{2\pi}{N-1}k}\}+2\text{Re}\{B_2\bar{h}^*[0]\bar{h}[2]e^{-j\frac{4\pi}{N-1}k}\}\Big) \quad (32)$$

where

$$\begin{aligned}
B_0 &= 48\left(3\sum_{l=0}^{2}\sum_{m=0}^{2}\left|\bar{h}[l]\right|^4\left|\bar{h}[m]\right|^2+6\prod_{l=0}^{2}\left|\bar{h}[l]\right|^2+\sum_{l=0}^{2}\left|\bar{h}[l]\right|^6\right)\\
B_{1_1} &= 32\sum_{l=0}^{2}\left|\bar{h}[l]\right|^4+64\left|\bar{h}[0]\right|^2\left|\bar{h}[2]\right|^2+80\left|\bar{h}[0]\right|^2\left|\bar{h}[1]\right|^2+96\left|\bar{h}[1]\right|^2\left|\bar{h}[2]\right|^2\\
B_{1_2} &= 32\sum_{l=0}^{2}\left|\bar{h}[l]\right|^4+128\left|\bar{h}[0]\right|^2\left|\bar{h}[2]\right|^2+32\left|\bar{h}[0]\right|^2\left|\bar{h}[1]\right|^2+80\left|\bar{h}[1]\right|^2\left|\bar{h}[2]\right|^2\\
B_2 &= 32\sum_{l=0}^{2}\left|\bar{h}[l]\right|^4+64\left(\left|\bar{h}[0]\right|^2\left|\bar{h}[1]\right|^2+\left|\bar{h}[1]\right|^2\left|\bar{h}[2]\right|^2\right)+80\left|\bar{h}[0]\right|^2\left|\bar{h}[2]\right|^2. \quad (33)
\end{aligned}$$

REFERENCES

[1] P.-I. Mak, S.-P. U, and R. Martins, "Transceiver architecture selection: Review, state-of-the-art survey and case study," *IEEE Circuits Syst. Mag.*, vol. 7, no. 2, pp. 6–25, 2nd Quarter, 2007.

[2] *IEEE Standard for Local and Metropolitan Area Networks Part 16: Air Interface for Fixed and Mobile Broadband Wireless Access Systems—Amendment 2: Physical and Medium Access Control Layers for Combined Fixed and Mobile Operation in Licensed Bands*, IEEE Std. 802.16e–2005, Feb. 2006.

[3] J. Vuolevi and T. Rahkonen, *Distortion in RF Power Amplifiers*. Norwood, MA, USA: Artech House, 2003.

[4] D. Petrovic, W. Rave, and G. Fettweis, "Effects of phase noise on OFDM systems with and without PLL: Characterization and compensation," *IEEE Trans. Commun.*, vol. 55, no. 8, pp. 1607–1616, Aug. 2007.

[5] A. Tarighat, R. Bagheri, and A. H. Sayed, "Compensation schemes and performance analysis of IQ imbalances in OFDM receivers," *IEEE Trans. Signal Process.*, vol. 53, no. 8, pp. 3257–3268, Aug. 2005.

[6] "Evolved Universal Terrestrial Radio Access (E-UTRA); User equipment (UE) radio transmission and reception," Sophia Antipolis, France, 3GPP Tech. spec. 36.101, ver. 8.3.0, Rel. 8, Sep. 2008.

[7] H. Zareian and V. Vakili, "Analytical EVM, BER, and TD performances of the OFDM systems in the presence of jointly nonlinear distortion and IQ imbalance," *Ann. Telecommun.*, vol. 64, no. 11/12, pp. 753–762, Dec. 2009.

[8] A. Georgiadis, "Gain, phase imbalance, and phase noise effects on error vector magnitude," *IEEE Trans. Veh. Technol.*, vol. 53, no. 2, pp. 443–449, Mar. 2004.

[9] C. Zhao and R. Baxley, "Error vector magnitude analysis for OFDM systems," in *Proc. 40th ACSSC*, Oct. 29, 2006/Nov. 1, 2006, pp. 1830–1834.

[10] P. Banelli and S. Capocardi, "Theoretical analysis and performance of OFDM signals in nonlinear AWGN channels," *IEEE Trans. Commun.*, vol. 48, no. 3, pp. 430–441, Mar. 2000.

[11] S. Wu and Y. Bar-Ness, "OFDM systems in the presence of phase noise: Consequences and solutions," *IEEE Trans. Commun.*, vol. 52, no. 11, pp. 1988–1996, Nov. 2004.

[12] T. Pollet, M. V. Bladel, and M. Moeneclaey, "BER sensitivity of OFDM systems to carrier frequency offset and Wiener phase noise," *IEEE Trans. Commun.*, vol. 43, no. 234, pp. 191–193, Feb./Mar./Apr. 1995.

[13] B. Priyanto, T. Sorensen, O. Jensen, T. Larsen, T. Kolding, and P. Mogensen, "Assessing and modeling the effect of RF impairments on UTRA LTE Uplink performance," in *Proc. IEEE 66th VTC-Fall*, Sep. 2007, pp. 1213–1217.

[14] T. C. W. Schenk and E. R. Fledderus, "RF Impairments in high-rate wireless systems—understanding the impact of TX/RX-asymmetry (invited)," in *Proc. 3rd Int. Symp. ISCCSP*, St. Julians, Malta, Mar. 2008, pp. 117–122.

[15] Y. Zou, M. Valkama, and M. Renfors, "Analysis and compensation of transmitter and receiver I/Q imbalances in space–time coded multiantenna OFDM systems," *EURASIP J. Wireless Commun. Netw.*, vol. 2008, no. 1, p. 391 025, Nov. 2007.

[16] C.-L. Liu, "Impacts of I/Q imbalance on QPSK-OFDM-QAM detection," *IEEE Trans. Consum. Electron.*, vol. 44, no. 3, pp. 984–989, Aug. 1998.

[17] H.-G. Ryu, Y. S. Li, and J.-S. Park, "Nonlinear analysis of the phase noise in the OFDM communication system," *IEEE Trans. Consum. Electron.*, vol. 50, no. 1, pp. 54–63, Feb. 2004.

[18] D. Morgan, Z. Ma, J. Kim, M. Zierdt, and J. Pastalan, "A generalized memory polynomial model for digital predistortion of RF power amplifiers," *IEEE Trans. Signal Process.*, vol. 54, no. 10, pp. 3852–3860, Oct. 2006.

[19] J. Minkoff, "The role of AM-to-PM conversion in memoryless nonlinear systems," *IEEE Trans. Commun.*, vol. COM-33, no. 2, pp. 139–144, Feb. 1985.

[20] "Evolved Universal Terrestrial Radio Access (E-UTRA); Base Station (BS) Radio Transmission and Reception," Sophia Antipolis, France, 3GPP TS 36.104 ver. 10.7.0, Rel. 10, Jul. 2012.

[21] P. Mathecken, T. Riihonen, S. Werner, and R. Wichman, "Performance analysis of OFDM with Wiener phase noise and frequency selective fading channel," *IEEE Trans. Commun.*, vol. 59, no. 5, pp. 1321–1331, May 2011.

[22] P. Mathecken, T. Riihonen, N. N. Tchamov, S. Werner, M. Valkama, and R. Wichman, "Characterization of OFDM radio link under PLL-based oscillator phase noise and multipath fading channel," *IEEE Trans. Commun.*, vol. 60, no. 6, pp. 1479–1485, Jun. 2012.

[23] C. Muschallik, "Influence of RF oscillators on an OFDM signal," *IEEE Trans. Consum. Electron.*, vol. 41, no. 3, pp. 592–603, Aug. 1995.

[24] J. Stott, "The effects of phase noise in COFDM," in *Proc. COFDM, BBC Res. Develop. Tech. Rev.*, Summer 1998, pp. 1–22.

[25] K. Fazel and S. Kaiser, *Multi-Carrier and Spread Spectrum Systems. From OFDM and MC-CDMA to LTE and WiMAX*, 2nd ed. Hoboken, NJ, USA: Wiley, 2008.

[26] I. Gradshteyn and I. Ryzhik, *Table of Integrals, Series and Products*. New York, NY, USA: Academic, 1994.

[27] R. Raich, H. Qian, and G. T. Zhou, "Orthogonal polynomials for power amplifier modeling and predistorter design," *IEEE Trans. Veh. Technol.*, vol. 53, no. 5, pp. 1468–1479, Sep. 2004.

[28] M. Bruno, J. Cousseau, A. Ghadam, and M. Valkama, "On high linearity high efficiency RF amplifier design," in *Proc. Argentine School Micro Nanoelectron. Technol. Appl.*, Oct. 2010, pp. 97–102.

[29] W. Kester, "Converting Oscillator Phase Noise to Time Jitter," Analog Devices Inc., Norwood, MA, USA, Tutorial MT-008, 2008.

[30] C. Masse and Q. Luu, "A 2.4 GHz WiMAX Direct Conversion Transmitter," Analog Devices Inc., Norwood, MA, USA, AN-826 Appl. Note, 2007.

[31] Hittite Microw. Corp., Chelmsford, MA, USA. [Online]. Available: http://www.hittite.com